bioRxiv preprint doi: https://doi.org/10.1101/2020.10.15.340703; this version posted October 15, 2020. The copyright holder for this preprint (which was not certified by peer review) is the author/funder, who has granted bioRxiv a license to display the preprint in perpetuity. It is made available under aCC-BY 4.0 International license.

Foxc1 establishes enhancer accessibility for craniofacial cartilage differentiation

Pengfei Xu[#], Haoze Vincent Yu[#], Kuo-Chang Tseng, Mackenzie Flath, Peter Fabian, Neil Segil and J. Gage Crump*

Eli and Edythe Broad Center for Regenerative Medicine, Department of Stem Cell Biology and Regenerative Medicine, Keck School of Medicine, University of Southern California, Los Angeles, CA 90033, USA

*Correspondence: J. Gage Crump, gcrump@usc.edu, (323) 442-2693

[#]These authors contributed equally

Highlights

- Dynamic chromatin accessibility across facial cartilage development
- Co-enrichment of Fox- and Sox-binding motifs in accessible regions
- Foxc1 establishes accessibility in a subset of facial cartilage enhancers
- Modular activity of Foxc1-dependent cartilage enhancers in zebrafish

bioRxiv preprint doi: https://doi.org/10.1101/2020.10.15.340703; this version posted October 15, 2020. The copyright holder for this preprint (which was not certified by peer review) is the author/funder, who has granted bioRxiv a license to display the preprint in perpetuity. It is made available under aCC-BY 4.0 International license.

Abstract

The specification of cartilage requires Sox9, a transcription factor with broad roles for organogenesis outside the skeletal system. How Sox9 gains selective access to cartilage-specific cis-regulatory regions during skeletal development had remained unclear. By analyzing chromatin accessibility during the differentiation of neural crest cells into chondrocytes of the zebrafish head, we find that cartilage-associated chromatin accessibility is dynamically established. Cartilage-associated regions that become accessible after neural crest migration are co-enriched for Sox9 and Fox transcription factor binding motifs. In zebrafish lacking Foxc1 paralogs, we find a global decrease in chromatin accessibility in chondrocytes, consistent with a later loss of dorsal facial cartilages. Zebrafish transgenesis assays confirm that many of these Foxc1-dependent elements function as enhancers with region- and stage-specific activity in facial cartilages. We propose that Foxc1-dependent chromatin accessibility helps directs the versatile Sox9 protein to a chondrogenic program in the face.

Introduction

bioRxiv preprint doi: https://doi.org/10.1101/2020.10.15.340703; this version posted October 15, 2020. The copyright holder for this preprint (which was not certified by peer review) is the author/funder, who has granted bioRxiv a license to display the preprint in perpetuity. It is made available under aCC-BY 4.0 International license.

Cartilage is the first skeletal type to be specified in the vertebrate body, providing important templates for later bone development and providing flexibility at joint surfaces and within the nose, ear, ribs, and larynx. The transcription factor Sox9 is essential for chondrogenic differentiation in all vertebrates examined (Lefebvre et al., 1997; Bi et al., 1999; Mori-Akiyama et al., 2003; Yan et al., 2005), yet it also has widespread roles outside the skeletal system, including in the reproductive system, kidney, liver, and skin (Jo et al., 2014). How Sox9 is directed to a chondrogenic program in trunk mesoderm and cranial neural crest-derived cells (CNCCs) has remained unclear. Sox9 is known to directly bind to a number of cis-regulatory elements adjacent to chondrogenic genes, including *Col2a1*, *Col10a1*, and *Acan* (Lefebvre et al., 1997; Dy et al., 2012; Askary et al., 2015; Ohba et al., 2015). However, it is not required for chromatin accessibility at these same elements (Liu et al., 2018), suggesting other unknown factors may first open chromatin at chondrogenic enhancers for later activation by Sox9.

Forkhead-domain (Fox) family transcription factors are excellent candidates for making chondrogenic enhancers accessible for later Sox9 activation. In the endoderm lineage, HNF3/FoxA binds closed chromatin at enhancers and makes these more accessible (Cirillo et

bioRxiv preprint doi: https://doi.org/10.1101/2020.10.15.340703; this version posted October 15, 2020. The copyright holder for this preprint (which was not certified by peer review) is the author/funder, who has granted bioRxiv a license to display the preprint in perpetuity. It is made available under aCC-BY 4.0 International license.

al., 2002). A similar chromatin accessibility role for Foxd3 in the early neural crest lineage has also been proposed (Lukoseviciute et al., 2018). In mice, loss of *Foxc1* results in widespread cartilage and bone defects (Kume et al., 1998), including impaired tracheal and rib cartilages (Hong et al., 1999), loss of calvarial bone due to premature ossification (Rice et al., 2003; Vivatbutsiri et al., 2008; Sun et al., 2013), syngnathia (Inman et al., 2013), and disruption of endochondral bone maturation (Yoshida et al., 2015). In zebrafish, loss of both Foxc1 paralogs (*foxc1a* and *foxc1b*) results in severe reductions of dorsal cartilages of the upper face, which are preceded by reduced expression of several Sox9 targets, including *col2a1a*, *acana*, *matn1*, and *matn4* (Xu et al., 2018). Chromatin immunoprecipitation followed by deep sequencing (ChIP-Seq) using a Sox9 antibody in dissected mouse rib and nose cartilage revealed enrichment of Fox binding motifs within Sox9-bound cis-regulatory sequences near chondrogenic genes (Ohba et al., 2015). Here, we use profiling of chromatin accessibility in wild-type and mutant zebrafish facial cartilages and find that Foxc1 paralogs are required for accessibility and activity of a number of cartilage enhancers. These findings support a model by which Foxc1 restricts Sox9 activity to a chondrogenic program by establishing selective accessibility of cartilage enhancers in CNCC-derived mesenchyme.

bioRxiv preprint doi: https://doi.org/10.1101/2020.10.15.340703; this version posted October 15, 2020. The copyright holder for this preprint (which was not certified by peer review) is the author/funder, who has granted bioRxiv a license to display the preprint in perpetuity. It is made available under aCC-BY 4.0 International license.

Results and Discussion

Chromatin accessibility landscape in chondrocytes of the zebrafish face

In order to identify potential cis-regulatory elements important for facial cartilage development, we performed a genome-wide analysis of chromatin accessibility in chondrocytes from 72 hours post-fertilization (hpf) zebrafish. We labeled chondrocytes by co-expression of *sox10:Dsred* and *col2a1a*:*GFP* transgenes (Figure 1A) and isolated double-positive and control double-negative cells by fluorescence-activated cell sorting (FACS). We then subjected these cells to a modified "micro" version of the assay for transposase accessible chromatin followed by next-generation sequencing (μATACseq). In order to focus on potential distal cis-regulatory elements, we excluded accessible regions within 1kb upstream or 0.5 kb downstream of transcription start sites. This analysis yielded 33,679 distal accessible elements, with 5,736 elements over-enriched in chondrocytes and 8,955 elements under-enriched in chondrocytes (Figure 1B-C). As confirmation of sequence quality, the cartilage-specific R2 enhancer of the Collagen Type II alpha 1 a gene (*col2a1a*) is enriched in chondrocyte-specific elements (Figure 1-figure supplement 1A). De novo motif analysis of the top 2000 chondrocyte-enriched regions using HOMER recovered motifs for Sox, Fox, Nfat, Zfx and Nkx transcription factor families (Figure

bioRxiv preprint doi: https://doi.org/10.1101/2020.10.15.340703; this version posted October 15, 2020. The copyright holder for this preprint (which was not certified by peer review) is the author/funder, who has granted bioRxiv a license to display the preprint in perpetuity. It is made available under aCC-BY 4.0 International license.

1D; Supplementary file 1A). Sox9 ChIP-Seq of mouse chondrocytes had previously revealed Nfat and Fox motifs as the second and third most co-enriched with Sox motifs (Ohba et al., 2015), and the Nkx motif might reflect the role of Nkx3.2 in cartilage differentiation (Provot et al., 2006). Consensus sequences for Sox, Fox, and Nfat motifs were highly similar between zebrafish and mouse (Figure 1-figure supplement 1B), despite our zebrafish analysis focusing on all accessible regions in facial chondrocytes and mouse analysis focusing on only Sox9-bound regions in rib chondrocytes. These striking motif similarities indicate strong conservation of the cartilage gene regulatory network between fish and mammals, and between the face and rib, and strongly suggest that many of the identified chondrocyte-specific accessible regions in zebrafish likely function as chondrocyte enhancers. In addition, Gene Ontology (GO) analysis of the nearest genes to the chondrocyte-enriched elements revealed cartilage development as one of the top 6 associated terms (Figure 1E). We also recovered terms for neural crest cell migration and dorsal/ventral pattern formation, likely reflecting retention of enhancer accessibility linked to the neural crest origins and later dorsoventral arch patterning of the precursors of facial cartilage.

bioRxiv preprint doi: https://doi.org/10.1101/2020.10.15.340703; this version posted October 15, 2020. The copyright holder for this preprint (which was not certified by peer review) is the author/funder, who has granted bioRxiv a license to display the preprint in perpetuity. It is made available under aCC-BY 4.0 International license.

97 **Progressive establishment of cartilage-associated chromatin accessibility**

98 We next investigated when cartilage-associated chromatin accessibility is established in relation
99 to CNCC development. CNCCs are first specified at ~10.5 hpf at the border of the neural keel,
100 finish their migration into the pharyngeal arches by ~20 hpf, and then show the first histological
101 signs of cartilage development in the jaw at ~52 hpf (Schilling and Kimmel, 1997). CNCC-
102 derived arch ectomesenchyme cells can be uniquely identified by co-expression of *fli1a:GFP*
103 and *sox10:Dsred* transgenes at 36 hpf and 48 hpf (Askary et al., 2017), stages just prior to
104 cartilage differentiation (Figure 2A). We performed μATACseq on *fli1a:GFP*+; *sox10:Dsred*+
105 cells after FACS and analyzed chondrocyte-specific accessible elements from our 72 hpf
106 dataset for their accessibilities at 36 and 48 hpf (Figure 2B). Of the 5,736 elements enriched in
107 chondrocytes at 72 hpf, only 6% (356) had peak accessibility at 36 hpf with no further increase
108 in accessibility by 48 hpf ("Group I"). In contrast, 48% (2,741) displayed increased accessibility
109 between 36 and 48 hpf ("Group II"), and 46% (2,639) between 48 and 72 hpf ("Group III"). For
110 Group I, de novo motif enrichment revealed predicted binding sites for members of the Nfat,
111 Fox, Lhx, Nr2f, Meis and Pax families, and significant GO terms included neural crest migration,
112 cell migration in general, and dorsal/ventral pattern formation (Figure 2C,D). Combined with the

bioRxiv preprint doi: https://doi.org/10.1101/2020.10.15.340703; this version posted October 15, 2020. The copyright holder for this preprint (which was not certified by peer review) is the author/funder, who has granted bioRxiv a license to display the preprint in perpetuity. It is made available under aCC-BY 4.0 International license.

known involvement of Foxd3 (Montero-Balaguer et al., 2006; Stewart et al., 2006), Lhx6/8 (Denaxa et al., 2009), Nr2f1/2/5 (Barske et al., 2018), Meis2 (Machon et al., 2015) and Pax9 (Nakatomi et al., 2010) in CNCC specification, migration, and dorsal-ventral arch patterning, many Group I elements likely represent retention of cis-regulatory elements involved in the earlier specification, migration, and regional patterning of CNCCs. Group II and Group III elements share many common predicted transcription factor binding motifs, including Sox dimer, Fox, Nfat, and Ap1 motifs previously described for mouse cartilage (Figure 2E,G; Supplementary file 1B) (Ohba et al., 2015). An Nkx motif was recovered only for Group II ($p=10^{-58}$, 36% of targets), an Egr motif was enriched for Group II ($p=10^{-65}$, 55% of targets) versus Group III ($p=10^{-20}$, 16% of targets), and a Tead motif was enriched for Group III ($p=10^{-63}$, 36% of targets) versus Group II ($p=10^{-20}$, 3% of targets). GO analysis for linked genes also revealed terms related to skeletal system development (Group II) and cartilage development (Group III), as well as more general terms such as transcription and organism development (Figure 2F,H). We therefore conclude that the majority of chondrocyte-specific elements gain accessibility after pharyngeal arch formation, and that transcription factor binding motifs change during cartilage differentiation. For example, enrichment of Nkx motifs in Group II elements might reflect the role

bioRxiv preprint doi: https://doi.org/10.1101/2020.10.15.340703; this version posted October 15, 2020. The copyright holder for this preprint (which was not certified by peer review) is the author/funder, who has granted bioRxiv a license to display the preprint in perpetuity. It is made available under aCC-BY 4.0 International license.

129 of Nkx3.2 in limiting chondrocyte maturation (Provot et al., 2006) and promoting joint formation

130 (Miller et al., 2003), while the preferential enrichment of the Tead motif, which is linked to

131 growth-associated Hippo signaling (Ota and Sasaki, 2008), in Group III elements might reflect

132 the later proliferative expansion of chondrocytes.

133

134 **Requirement of Foxc1 for chromatin accessibility at a subset of cartilage elements**

135 We had previously found that Foxc1 genes are essential for cartilage development in the upper

136 face (Xu et al., 2018), and both our μATACseq analysis of zebrafish chondrocytes and

137 published Sox9 ChIP-seq analysis in mouse (Ohba et al., 2015) reveals co-enrichment of Sox

138 and Fox motifs in accessible regions near known cartilage genes. In zebrafish Foxc1 (*foxc1a-/-;*

139 *foxc1b-/-*) mutants, cartilages of the upper/dorsal face fail to develop (Xu et al., 2018). In order

140 to isolate the dorsal CNCC precursors affected in Foxc1 mutants, we used a *pou3f3b:Gal4*;

141 *UAS:nlsGFP* (*pou3f3b>GFP*) dorsal CNCC transgenic line (#Barske et al., 2020, PNAS, in

142 press) along with the pan-CNCC *sox10:Dsred* transgenic line. Whereas *pou3f3b>GFP+;*

143 *sox10:Dsred*+ CNCCs were present in Foxc1 mutant pharyngeal arches at 48 hpf, many fewer

144 differentiated into chondrocytes by 6 days post-fertilization (dpf) compared to sibling controls

bioRxiv preprint doi: https://doi.org/10.1101/2020.10.15.340703; this version posted October 15, 2020. The copyright holder for this preprint (which was not certified by peer review) is the author/funder, who has granted bioRxiv a license to display the preprint in perpetuity. It is made available under aCC-BY 4.0 International license.

(Figure 3A-D). We therefore performed μATACseq on *pou3f3b>GFP+; sox10:Dsred+* cells after FACS from Foxc1 mutants and controls at 36 and 48 hpf. A comparison of the 15,781 accessible regions in dorsal CNCCs (*pou3f3b>GFP+; sox10:Dsred+*) and pan-CNCCs (*fli1a:GFP+; sox10:Dsred+*) at 36 hpf revealed 79% with similar accessibility, 11% with greater accessibility in dorsal CNCCs, and 10% with greater accessibility in pan-CNCCs (Figure 3-figure supplement 1A). Of 22,323 elements at 48 hpf, 72% were similarly accessible, 10% more accessible in dorsal CNCCs, and 18% more accessible in pan-CNCCs (Figure 3-figure supplement 1B). A comparison of the 5,736 regions with specific accessibility in cartilage at 72 hpf revealed high correlation between dorsal- and pan-CNCCs at 36 hpf, with 96% displaying similar accessibility (r=0.92, Figure 3-figure supplement 2A,C). By 48 hpf, however, we observed notable differences between accessibility of cartilage-specific elements, with 43% displaying greater accessibility in pan-CNCCs and only 0.2% displaying greater accessibility in dorsal CNCCs (r=0.71, Figure 3-figure supplement 2B,D). The decreased accessibility of cartilage-specific elements in dorsal CNCCs at 48 hpf supports previous studies that dorsal chondrocytes develop later than other chondrocytes in the zebrafish face (Schilling and Kimmel, 1997; Barske et al., 2016).

bioRxiv preprint doi: https://doi.org/10.1101/2020.10.15.340703; this version posted October 15, 2020. The copyright holder for this preprint (which was not certified by peer review) is the author/funder, who has granted bioRxiv a license to display the preprint in perpetuity. It is made available under aCC-BY 4.0 International license.

Analysis of cartilage-associated elements in Foxc1 mutants revealed that 10% (120/1,221) of elements that have established peak accessibility by 36 hpf (i.e. Group I) and 41% (636/1,556) of elements that increase accessibility between 36 and 48 hpf (i.e. Group II) had reduced accessibility in Foxc1 mutants (Figure 3E). De novo motif analysis of Foxc1-dependent and Foxc1-independent elements in Group I showed enrichment of Sox ($p=10^{-12}$, $p=10^{-76}$), Tead ($p=10^{-14}$, $p=10^{-20}$) Mtf ($p=10^{-12}$, $p=10^{-22}$) and Ets ($p=10^{-12}$, $p=10^{-61}$) motifs in both (Figure 3F, Supplementary file 1C). Whereas Fox motifs were uncovered in both, a closer analysis revealed enrichment of Foxa2 and Foxd3 motifs only in Foxc1-dependent elements ($p=10^{-45}$, 38% of targets; $p=10^{-16}$, 18% of targets), and a Foxo1 motif only in Foxc1-independent elements ($p=10^{-42}$, 49% of targets). Similarly in Group II elements, a Foxa1 motif was enriched only in Foxc1-dependent elements ($p=10^{-59}$, 38% of targets), and Foxh1 and Foxp1 motifs only in Foxc1-independent elements ($p=10^{-22}$, 22% of targets; $p=10^{-19}$, 7% of targets) (Figure 3G, Supplementary file 1C). Although Foxc1 motifs were not in the database used for motif predictions, the selective presence of Foxa1/2 motifs in Foxc1-dependent elements is consistent with previous reports that the consensus sequence for Foxc1-bound peaks is nearly identical to Foxa1/2 motifs (Wang et al., 2016). Sox motifs were similarly enriched in both Group I and

bioRxiv preprint doi: https://doi.org/10.1101/2020.10.15.340703; this version posted October 15, 2020. The copyright holder for this preprint (which was not certified by peer review) is the author/funder, who has granted bioRxiv a license to display the preprint in perpetuity. It is made available under aCC-BY 4.0 International license.

Group II Foxc1-dependent and -independent elements, and Nfat and Zfx motifs in Group II Foxc1-dependent and -independent elements. An Insm (p=10^{-39}, 30% of targets) motif was uncovered only in Foxc1-independent Group I elements, and an Nkx motif (p=10^{-35}, 52% of targets) only in Foxc1-independent Group II elements. These findings suggest that Foxc1-dependent and -independent cartilage elements are commonly bound by Sox9 but likely differ in co-binding by Foxc1 and additional co-factors. For example, the presence of the Nkx motif only in Foxc1-independent elements suggests that it could be an alternative co-factor for Sox9, in line with the known roles for Nkx3.2 in chondrocyte biology (Provot et al., 2006).

Validation of Foxc1-dependent cartilage enhancers in zebrafish transgenesis assays

To verify whether Foxc1-dependent cartilage elements identified by μATACseq are chondrogenic enhancers, we tested the ability of individual elements in combination with an E1b minimal promoter to drive cartilage expression of green fluorescent protein (GFP) in zebrafish transgenic assays (Figure 4-figure supplement 1A). We tested 22 Foxc1-dependent elements near 15 different genes, which included elements linked to genes with known cartilage function (*ucmab*, *matn4*, *matn1*, *lect1*, *epyc*, *col9a1a*, *col9a3*, *sox10*, *acana, foxa3*, *mia*) and others with

bioRxiv preprint doi: https://doi.org/10.1101/2020.10.15.340703; this version posted October 15, 2020. The copyright holder for this preprint (which was not certified by peer review) is the author/funder, who has granted bioRxiv a license to display the preprint in perpetuity. It is made available under aCC-BY 4.0 International license.

193 unknown cartilage function (*si:dkey33i1l.4*, *gas1b*, *lefty2*, *slc35d1a*) (Figure 4A; Figure 4-figure

194 supplement 1; Supplementary file 2) . We observed that 59% (13/22) of elements drove GFP

195 expression in facial chondrocytes at 6 dpf. These included intronic elements within *sox10*, *lect1*,

196 *col9a3, col9a1a* and *slc35d1a*; distal 5' elements near *ucmab*, *epyc*, *mia, acana,* and *matn4*; a

197 distal 3' element near *gas1b*; and a promoter-associated element for *lect1*. All tested elements

198 are from Group II, i.e. increasing accessibility between 36 and 48 hpf, and we confirmed

199 cartilage expression in independent stable transgenic lines in 9 cases (Figure 4B; Figure 4-

200 figure supplement 1; Supplementary file 2). Whereas an element in the first intron of *sox10*

201 drove uniform cartilage-specific expression, most elements drove expression in specific sub-

202 regions or differentiation stages of facial chondrocytes. Whereas a distal 5' element of *ucmab*

203 drove expression in chondrocytes of multiple joints in the zebrafish head, an intronic element of

204 *lect1* drove chondrocyte expression only in the jaw joint and hyomandibular-otic connection, a

205 promoter-associated element of *lect1* drove expression more strongly in the hyoid joint and

206 hyomandibular-symplectic connection (though also more broadly in chondrocytes), and a distal

207 5' element of *acana* drove restricted chondrocyte expression at the hyoid joint. Reciprocally,

208 elements associated with *col9a3*, *epyc*, *mia*, and *col9a1a* were expressed in chondrocytes but

bioRxiv preprint doi: https://doi.org/10.1101/2020.10.15.340703; this version posted October 15, 2020. The copyright holder for this preprint (which was not certified by peer review) is the author/funder, who has granted bioRxiv a license to display the preprint in perpetuity. It is made available under aCC-BY 4.0 International license.

209 generally excluded from joint regions (particularly apparent at the hyoid joint and

210 hyomandibular-symplectic connection). Further, we found that three enhancer transgenes with

211 diverse expression patterns (broad *sox10*, joint-restricted *ucmab*, and joint-excluded *epyc*

212 enhancers) all displayed reduced activity specifically in the dorsal cartilage regions affected in

213 Foxc1 mutants (Figure 4C). We also tested four Foxc1-independent elements and found that

214 two drove cartilage expression (distal 5' elements of *gas1b* and *matn4*), one drove ligament

215 expression (distal 5' element of *sparc*), and one had no activity (promoter-associated element of

216 *sox10*) (Figure 4-figure supplement 1). Thus, the majority of accessible elements tested had

217 chondrocyte activity, and Foxc1-dependent and -independent elements appear equally capable

218 of driving cartilage expression. Moreover, the activity of different enhancers in diverse locations

219 and stages of chondrocyte maturation indicates that global cartilage expression patterns are

220 achieved in part through the summation of enhancers with more restricted activity.

221

222 **Conclusion**

223 Our findings indicate that Foxc1 function is required for the accessibility of close to half of

224 chondrocyte enhancers in the zebrafish face. Given expression and function of Foxc1 in diverse

bioRxiv preprint doi: https://doi.org/10.1101/2020.10.15.340703; this version posted October 15, 2020. The copyright holder for this preprint (which was not certified by peer review) is the author/funder, who has granted bioRxiv a license to display the preprint in perpetuity. It is made available under aCC-BY 4.0 International license.

cartilages (e.g. limb, rib, tracheal) in mouse, it seems likely that Foxc1 has a similar function in chondrocyte enhancer accessibility throughout the body. It is unclear why only a minority of enhancers appears to require Foxc1 activity. It is possible that other members of the Fox family compensate, such as Foxf1/2 in the facial midline (Xu et al., 2018) and Foxa2/3 during later hypertrophic maturation (Ionescu et al., 2012). Alternatively, there may be other co-factors that cooperate with Sox9 for chondrocyte enhancer accessibility and activation, such as Nkx3.2. We did not detect any obvious differences in the types of enhancer-proximal genes or the patterns and stages associated with Foxc1-dependent versus -independent enhancer activity. Further work will also be needed to understand the mechanism by which Foxc1 promotes chondrocyte enhancer accessibility. Foxc1 lacks a chromatin modifying domain (Yoshida et al., 2015) and therefore would need to interact with a co-factor to directly open chromatin. Foxc1 could also act to maintain open chromatin, as shown for Foxa1 in the liver (Reizel et al., 2020). Given that both Foxc1 and Sox9 have expression in many tissues outside the skeletal system, it will also be important to determine whether additional factors help to further restrict their activity to chondrocyte enhancers within skeletogenic mesenchyme.

bioRxiv preprint doi: https://doi.org/10.1101/2020.10.15.340703; this version posted October 15, 2020. The copyright holder for this preprint (which was not certified by peer review) is the author/funder, who has granted bioRxiv a license to display the preprint in perpetuity. It is made available under aCC-BY 4.0 International license.

241 **Methods**

242 ***Zebrafish lines***

243 The Institutional Animal Care and Use Committee of the University of Southern California

244 approved all experiments on zebrafish (*Danio rerio*) (Protocol #10885). Existing mutant and

245 transgenic lines used in this study include *foxc1a*^{el542} and *foxc1b*^{el620} (Xu et al., 2018);

246 Tg(*sox10:Dsred*)^{el110} and Tg(*fli1a:EGFP*)^{y1} (Askary et al., 2017); Tg(*col2a1aBAC:GFP*) (Paul et

247 al., 2016); and *Tg(UAS:nlsGFP;α-crystallin:Cerulean)*^{el609} *and pou3f3b*$^{Gal4ff\text{-}el79}$ (#Barske et al.,

248 2020, PNAS, in press). For enhancer transgenic lines, we synthesized accessible elements with

249 flanking attB4 and attB1 sequences using IDT gBlocks and cloned these into pDONR-P4-P1R

250 using the Gateway Tol2kit (Invitrogen) to create p5E enhancer constructs (Kwan et al., 2007).

251 We then combined p5E constructs with pME-E1b-GFP, p3E-polyA, and pDestTol2AB2 using LR

252 clonase. Final DNA constructs were microinjected with transposase RNA (30 ng/μl each) into 1-

253 cell stage zebrafish embryos. In most cases, multiple independent stable alleles per construct

254 were analyzed in the F1 generation (Supplementary file 2).

255

256 ***Confocal imaging***

bioRxiv preprint doi: https://doi.org/10.1101/2020.10.15.340703; this version posted October 15, 2020. The copyright holder for this preprint (which was not certified by peer review) is the author/funder, who has granted bioRxiv a license to display the preprint in perpetuity. It is made available under aCC-BY 4.0 International license.

257 Transgenic embryos were imaged with a Zeiss LSM800 confocal microscope. Maximum

258 intensity projections are shown for stable transgenic lines and single representative sections are

259 shown for injected embryos. Image levels were modified consistently across samples in Adobe

260 Photoshop CS6.

261

262 ***μATACseq***

263 Wild-type embryos double-positive for *fli1a:EGFP* and *sox10:Dsred* (36 hpf and 48 hpf), or

264 *col2a1a:GFP* and *sox10:Dserd* (72 hpf), were sorted under a fluorescent dissecting microscope

265 (Leica M165FC) before dissociation. For Foxc1 mutant analysis, we performed incrosses of

266 *pou3f3b:Gal4+/-*; *UAS:nls-GFP+/-*; *sox10:Dsred+/-*; *foxc1a+/-*; *foxc1b+/-* fish and then selected

267 for GFP+/Dsred+ embryos on a fluorescent dissecting microscope. Genotyping was then

268 performed on tail lysates collected from individual embryos at 27 hpf. We then pooled *foxc1a-/-*;

269 *foxc1b-/-* double mutants and separate sibling controls (*foxc1a*+/-; *foxc1b*+/+ and *foxc1a*+/+;

270 *foxc1b* +/+ embryos) for FACS. To facilitate embryo collection at the 36 hpf time point, embryos

271 were moved at 27 hpf to an incubator set at 22°C to delay their development such that they

272 reached 36 hpf the following morning. Cell dissociation and FACS were performed as previously

bioRxiv preprint doi: https://doi.org/10.1101/2020.10.15.340703; this version posted October 15, 2020. The copyright holder for this preprint (which was not certified by peer review) is the author/funder, who has granted bioRxiv a license to display the preprint in perpetuity. It is made available under aCC-BY 4.0 International license.

273 described (Askary et al., 2017). Around 5000 cells of each sample were centrifuged at 500 g for
274 20 m at 4 °C, and the pellet was suspended with 20 µL of lysis buffer (10 mM Tris HCl (pH 7.4),
275 5 mM $MgCl_2$, 10% DMF, 0.2% N-P40) by pipetting 6-10 times to release the nuclei without
276 purification. The cell lysate was then mixed with 30 µL reaction buffer (10 mM Tris HCl (pH 7.4),
277 5 mM $MgCl_2$, 10% DMF, and homemade Tn5 Transposase) by vortexing for 5 s. The reaction
278 was incubated at 37°C for 20 minutes, followed by DNA purification using a Qiagen MiniElute
279 kit. Purified DNA fragments were used to conduct µATACseq libraries as previously described
280 (Buenrostro et al., 2013) and sequenced using the NextSeq 500 platform (Illumina) with a
281 minimum of 50 million paired-reads/sample.
282
283 **Data analysis and statistics**
284 The Encode analysis pipeline (https://github.com/ENCODE-DCC/chip-seq-pipeline) for
285 ATACseq was used with small modifications. The raw reads were trimmed to 37 bp and aligned
286 to zebrafish GRCz10 genome assembly by STAR aligner (Dobin et al. 2013). PCR duplicates,
287 and the reads that aligned to “blacklist regions” (Amemiya et al. 2019) were removed, and then
288 peaks were called by Model-based analysis of ChIP-Seq (MACS2) (Zhang et al. 2008) with

bioRxiv preprint doi: https://doi.org/10.1101/2020.10.15.340703; this version posted October 15, 2020. The copyright holder for this preprint (which was not certified by peer review) is the author/funder, who has granted bioRxiv a license to display the preprint in perpetuity. It is made available under aCC-BY 4.0 International license.

289 *p*=0.01 cutoff and disabled dynamic lambda option (--nolambda) for individual replicates. Peaks
290 from individual replicates were further filtered by IDR<0.01, and the overlapping peaks between
291 replicates were used. Bigwig files were generated from dup-removed bam files with *bedtools*
292 and *bedgraphtobigwig*, and normalization was based on total read numbers. Heatmaps were
293 generated with DeepTools (Ramírez et al. 2016) based on the normalized bigwig signal files.
294 Individual genomic loci were examined by IGV (Broad Institute). Differential analyses of
295 μATACseq data was done with DESeq2 (Love et al. 2014). HOMER (Heinz et al. 2010) was
296 used to identify de novo motifs. David 6.8 GO analysis was performed on the web interface
297 (https://david.ncifcrf.gov/) based on nearest neighbor genes for all differentially accessible
298 elements. Pearson correlation was calculated using cor() function in R.
299

300 **Acknowledgements**

301 We thank Jeffrey Boyd at the USC Stem Cell Flow Cytometry Core for FACS, David Ruble at
302 the CHLA Sequencing Core, the high-performance computing core at USC, and Megan
303 Matsutani, Jennifer DeKoeyer Crump, and Mathi Thiruppathy for fish care. We dedicate this
304 work to the late Bartosz Balczerski whose passion as a postdoc inspired this project.

bioRxiv preprint doi: https://doi.org/10.1101/2020.10.15.340703; this version posted October 15, 2020. The copyright holder for this preprint (which was not certified by peer review) is the author/funder, who has granted bioRxiv a license to display the preprint in perpetuity. It is made available under aCC-BY 4.0 International license.

Author Contributions

P.X. and J.G.C. conceived of experiments. P.X., M.F, and P.F. conducted zebrafish experiments. P.X. and H.V.Y. performed μATACseq experiments, and with K.-C.T. conducted bioinformatics analysis. N.S. and J.G.C. obtained funding and oversaw project. P.X. and J.G.C. wrote the manuscript.

Competing interests

The authors declare no competing interests.

Materials & Correspondence

Requests for material should be directed to J. Gage Crump (gcrump@usc.edu).

Data availability

μATACseq data can be accessed at GEO with accession number GSE157575:

visit https://www.ncbi.nlm.nih.gov/geo/query/acc.cgi?acc=GSE157575__;!!LIr3w8kk_Xxm!4o2V xflwp2flZl1FVkwGRA5Q9CcHhvfeKfQYZftKgRy6JUHBaaAPO2btB-Xgs0o$ and enter token gzcxqyourvmdnuj into the box.

bioRxiv preprint doi: https://doi.org/10.1101/2020.10.15.340703; this version posted October 15, 2020. The copyright holder for this preprint (which was not certified by peer review) is the author/funder, who has granted bioRxiv a license to display the preprint in perpetuity. It is made available under aCC-BY 4.0 International license.

References

Askary, A., Xu, P., Barske, L., Bay, M., Bump, P., Balczerski, B., Bonaguidi, M. A. and Crump, J. G. (2017). Genome-wide analysis of facial skeletal regionalization in zebrafish. *Development* **144**, 2994-3005.

Askary, A., Mork, L., Paul, S., He, X., Izuhara, A. K., Gopalakrishnan, S., Ichida, J. K., McMahon, A. P., Dabizljevic, S., Dale, R. et al. (2015). Iroquois Proteins Promote Skeletal Joint Formation by Maintaining Chondrocytes in an Immature State. *Dev Cell* **35**, 358-365.

Barske, L., Rataud, P., Behizad, K., Del Rio, L., Cox, S. G. and Crump, J. G. (2018). Essential Role of Nr2f Nuclear Receptors in Patterning the Vertebrate Upper Jaw. *Dev Cell* **44**, 337-347 e335.

Barske, L., Askary, A., Zuniga, E., Balczerski, B., Bump, P., Nichols, J. T. and Crump, J. G. (2016). Competition between Jagged-Notch and Endothelin1 Signaling Selectively Restricts Cartilage Formation in the Zebrafish Upper Face. *PLoS Genet* **12**, e1005967.

Bi, W., Deng, J. M., Zhang, Z., Behringer, R. R. and de Crombrugghe, B. (1999). Sox9 is required for cartilage formation. *Nat Genet* **22**, 85-89.

Buenrostro, J. D., Giresi, P. G., Zaba, L. C., Chang, H. Y. and Greenleaf, W. J. (2013). Transposition of native chromatin for fast and sensitive epigenomic profiling of open chromatin, DNA-binding proteins and nucleosome position. *Nat Methods* **10**, 1213-1218.

Cirillo, L. A., Lin, F. R., Cuesta, I., Friedman, D., Jarnik, M. and Zaret, K. S. (2002). Opening of compacted chromatin by early developmental transcription factors HNF3 (FoxA) and GATA-4. *Mol Cell* **9**, 279-289.

Denaxa, M., Sharpe, P. T. and Pachnis, V. (2009). The LIM homeodomain transcription factors Lhx6 and Lhx7 are key regulators of mammalian dentition. *Dev Biol* **333**, 324-336.

Dy, P., Wang, W., Bhattaram, P., Wang, Q., Wang, L., Ballock, R. T. and Lefebvre, V. (2012). Sox9 directs hypertrophic maturation and blocks osteoblast differentiation of growth plate chondrocytes. *Dev Cell* **22**, 597-609.

Hong, H. K., Lass, J. H. and Chakravarti, A. (1999). Pleiotropic skeletal and ocular phenotypes of the mouse mutation congenital hydrocephalus (ch/Mf1) arise from a winged helix/forkhead transcriptionfactor gene. *Hum Mol Genet* **8**, 625-637.

bioRxiv preprint doi: https://doi.org/10.1101/2020.10.15.340703; this version posted October 15, 2020. The copyright holder for this preprint (which was not certified by peer review) is the author/funder, who has granted bioRxiv a license to display the preprint in perpetuity. It is made available under aCC-BY 4.0 International license.

Inman, K. E., Purcell, P., Kume, T. and Trainor, P. A. (2013). Interaction between Foxc1 and Fgf8 during mammalian jaw patterning and in the pathogenesis of syngnathia. *PLoS Genet* **9**, e1003949.

Ionescu, A., Kozhemyakina, E., Nicolae, C., Kaestner, K. H., Olsen, B. R. and Lassar, A. B. (2012). FoxA family members are crucial regulators of the hypertrophic chondrocyte differentiation program. *Dev Cell* **22**, 927-939.

Jo, A., Denduluri, S., Zhang, B., Wang, Z., Yin, L., Yan, Z., Kang, R., Shi, L. L., Mok, J., Lee, M. J. et al. (2014). The versatile functions of Sox9 in development, stem cells, and human diseases. *Genes Dis* **1**, 149-161.

Kume, T., Deng, K. Y., Winfrey, V., Gould, D. B., Walter, M. A. and Hogan, B. L. (1998). The forkhead/winged helix gene Mf1 is disrupted in the pleiotropic mouse mutation congenital hydrocephalus. *Cell* **93**, 985-996.

Kwan, K. M., Fujimoto, E., Grabher, C., Mangum, B. D., Hardy, M. E., Campbell, D. S., Parant, J. M., Yost, H. J., Kanki, J. P. and Chien, C. B. (2007). The Tol2kit: a multisite gateway-based construction kit for Tol2 transposon transgenesis constructs. *Dev Dyn* **236**, 3088-3099.

Lefebvre, V., Huang, W., Harley, V. R., Goodfellow, P. N. and de Crombrugghe, B. (1997). SOX9 is a potent activator of the chondrocyte-specific enhancer of the pro alpha1(II) collagen gene. *Mol Cell Biol* **17**, 2336-2346.

Liu, C. F., Angelozzi, M., Haseeb, A. and Lefebvre, V. (2018). SOX9 is dispensable for the initiation of epigenetic remodeling and the activation of marker genes at the onset of chondrogenesis. *Development* **145**.

Lukoseviciute, M., Gavriouchkina, D., Williams, R. M., Hochgreb-Hagele, T., Senanayake, U., Chong-Morrison, V., Thongjuea, S., Repapi, E., Mead, A. and Sauka-Spengler, T. (2018). From Pioneer to Repressor: Bimodal foxd3 Activity Dynamically Remodels Neural Crest Regulatory Landscape In Vivo. *Dev Cell* **47**, 608-628 e606.

Machon, O., Masek, J., Machonova, O., Krauss, S. and Kozmik, Z. (2015). Meis2 is essential for cranial and cardiac neural crest development. *BMC Dev Biol* **15**, 40.

Miller, C. T., Yelon, D., Stainier, D. Y. and Kimmel, C. B. (2003). Two endothelin 1 effectors, hand2 and bapx1, pattern ventral pharyngeal cartilage and the jaw joint. *Development* **130**, 1353-1365.

bioRxiv preprint doi: https://doi.org/10.1101/2020.10.15.340703; this version posted October 15, 2020. The copyright holder for this preprint (which was not certified by peer review) is the author/funder, who has granted bioRxiv a license to display the preprint in perpetuity. It is made available under aCC-BY 4.0 International license.

Montero-Balaguer, M., Lang, M. R., Sachdev, S. W., Knappmeyer, C., Stewart, R. A., De La Guardia, A., Hatzopoulos, A. K. and Knapik, E. W. (2006). The mother superior mutation ablates foxd3 activity in neural crest progenitor cells and depletes neural crest derivatives in zebrafish. *Dev Dyn* **235**, 3199-3212.

Mori-Akiyama, Y., Akiyama, H., Rowitch, D. H. and de Crombrugghe, B. (2003). Sox9 is required for determination of the chondrogenic cell lineage in the cranial neural crest. *Proc Natl Acad Sci U S A* **100**, 9360-9365.

Nakatomi, M., Wang, X. P., Key, D., Lund, J. J., Turbe-Doan, A., Kist, R., Aw, A., Chen, Y., Mass, R. L. and Peters, H. (2010). Genetic interactions between Pax9 and Msx1 regulate lip development and several stages of tooth morphogenesis. *Dev Biol* **340**, 438-449.

Ohba, S., He, X., Hojo, H. and McMahon, A. P. (2015). Distinct Transcriptional Programs Underlie Sox9 Regulation of the Mammalian Chondrocyte. *Cell Rep* **12**, 229-243.

Ota, M. and Sasaki, H. (2008). Mammalian Tead proteins regulate cell proliferation and contact inhibition as transcriptional mediators of Hippo signaling. *Development* **135**, 4059-4069.

Paul, S., Schindler, S., Giovannone, D., de Millo Terrazzani, A., Mariani, F. V. and Crump, J. G. (2016). Ihha induces hybrid cartilage-bone cells during zebrafish jawbone regeneration. *Development* **143**, 2066-2076.

Provot, S., Kempf, H., Murtaugh, L. C., Chung, U. I., Kim, D. W., Chyung, J., Kronenberg, H. M. and Lassar, A. B. (2006). Nkx3.2/Bapx1 acts as a negative regulator of chondrocyte maturation. *Development* **133**, 651-662.

Reizel, Y., Morgan, A., Gao, L., Lan, Y., Manduchi, E., Waite, E. L., Wang, A. W., Wells, A. and Kaestner, K. H. (2020). Collapse of the hepatic gene regulatory network in the absence of FoxA factors. *Genes Dev* **34**, 1039-1050.

Retting, K. N., Song, B., Yoon, B. S. and Lyons, K. M. (2009). BMP canonical Smad signaling through Smad1 and Smad5 is required for endochondral bone formation. *Development* **136**, 1093-1104.

Rice, R., Rice, D. P., Olsen, B. R. and Thesleff, I. (2003). Progression of calvarial bone development requires Foxc1 regulation of Msx2 and Alx4. *Dev Biol* **262**, 75-87.

Schilling, T. F. and Kimmel, C. B. (1997). Musculoskeletal patterning in the pharyngeal segments of the zebrafish embryo. *Development* **124**, 2945-2960.

bioRxiv preprint doi: https://doi.org/10.1101/2020.10.15.340703; this version posted October 15, 2020. The copyright holder for this preprint (which was not certified by peer review) is the author/funder, who has granted bioRxiv a license to display the preprint in perpetuity. It is made available under aCC-BY 4.0 International license.

411 **Stewart, R. A., Arduini, B. L., Berghmans, S., George, R. E., Kanki, J. P., Henion, P. D. and**
412 **Look, A. T.** (2006). Zebrafish foxd3 is selectively required for neural crest specification,
413 migration and survival. *Dev Biol* **292**, 174-188.
414 **Sun, J., Ishii, M., Ting, M. C. and Maxson, R.** (2013). Foxc1 controls the growth of the murine
415 frontal bone rudiment by direct regulation of a Bmp response threshold of Msx2.
416 *Development* **140**, 1034-1044.
417 **Vivatbutsiri, P., Ichinose, S., Hytonen, M., Sainio, K., Eto, K. and Iseki, S.** (2008). Impaired
418 meningeal development in association with apical expansion of calvarial bone osteogenesis
419 in the Foxc1 mutant. *J Anat* **212**, 603-611.
420 **Wang, L., Siegenthaler, J. A., Dowell, R. D. and Yi, R.** (2016). Foxc1 reinforces quiescence in
421 self-renewing hair follicle stem cells. *Science* **351**, 613-617.
422 **Xu, P., Balczerski, B., Ciozda, A., Louie, K., Oralova, V., Huysseune, A. and Crump, J. G.**
423 (2018). Fox proteins are modular competency factors for facial cartilage and tooth
424 specification. *Development* **145**.
425 **Yan, Y. L., Willoughby, J., Liu, D., Crump, J. G., Wilson, C., Miller, C. T., Singer, A.,**
426 **Kimmel, C., Westerfield, M. and Postlethwait, J. H.** (2005). A pair of Sox: distinct and
427 overlapping functions of zebrafish sox9 co-orthologs in craniofacial and pectoral fin
428 development. *Development* **132**, 1069-1083.
429 **Yoshida, M., Hata, K., Takashima, R., Ono, K., Nakamura, E., Takahata, Y., Murakami, T.,**
430 **Iseki, S., Takano-Yamamoto, T., Nishimura, R. et al.** (2015). The transcription factor
431 Foxc1 is necessary for Ihh-Gli2-regulated endochondral ossification. *Nat Commun* **6**, 6653.

bioRxiv preprint doi: https://doi.org/10.1101/2020.10.15.340703; this version posted October 15, 2020. The copyright holder for this preprint (which was not certified by peer review) is the author/funder, who has granted bioRxiv a license to display the preprint in perpetuity. It is made available under aCC-BY 4.0 International license.

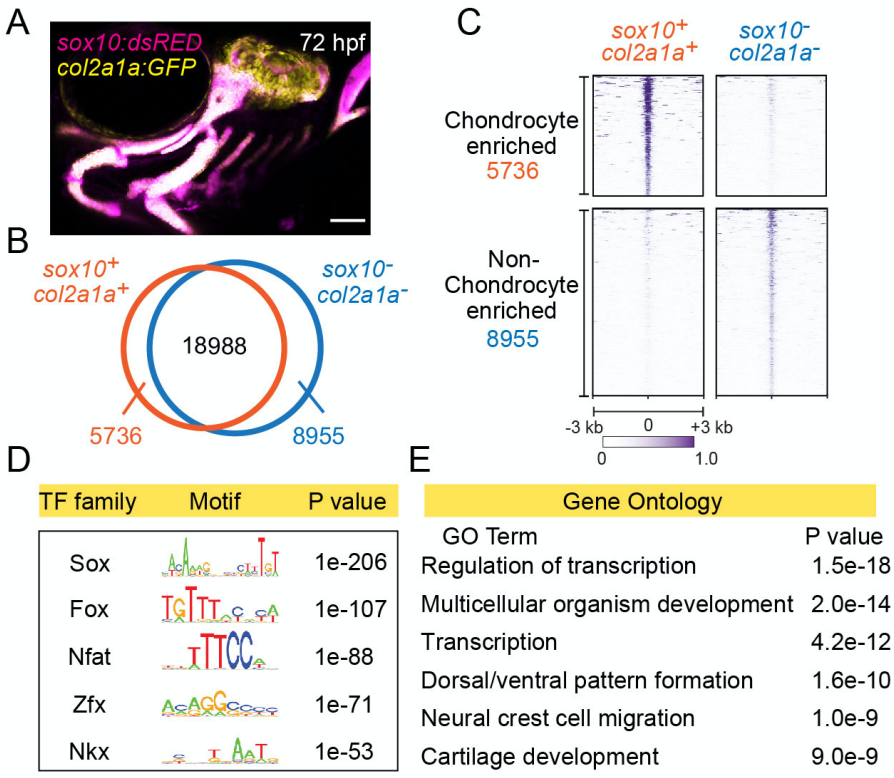

Figure 1. Chromatin accessibility landscape of facial chondrocytes

(A) Confocal image of facial cartilages expressing *col2a1a:GFP* and *sox10:Dsred* at 72 hpf. Lateral view with anterior to left. Scale bar = 100 μm. (B) Venn diagram indicating distal elements with open chromatin accessibility in *col2a1a:GFP*+; *sox10:Dsred*+ versus *col2a1a:GFP*-; *sox10:Dsred*- cells. (C) Peak intensity plots (Heatmap) of μATACseq show differentially enriched open chromatin regions in double-positive versus double-negative cells. (D) The top 5 transcription factor (TF) motifs recovered from the top 2000 μATACseq peaks enriched in chondrocytes (after removing redundant motifs). (E) GO analysis of nearest neighbor genes of μATACseq peaks enriched in chondrocytes.

bioRxiv preprint doi: https://doi.org/10.1101/2020.10.15.340703; this version posted October 15, 2020. The copyright holder for this preprint (which was not certified by peer review) is the author/funder, who has granted bioRxiv a license to display the preprint in perpetuity. It is made available under aCC-BY 4.0 International license.

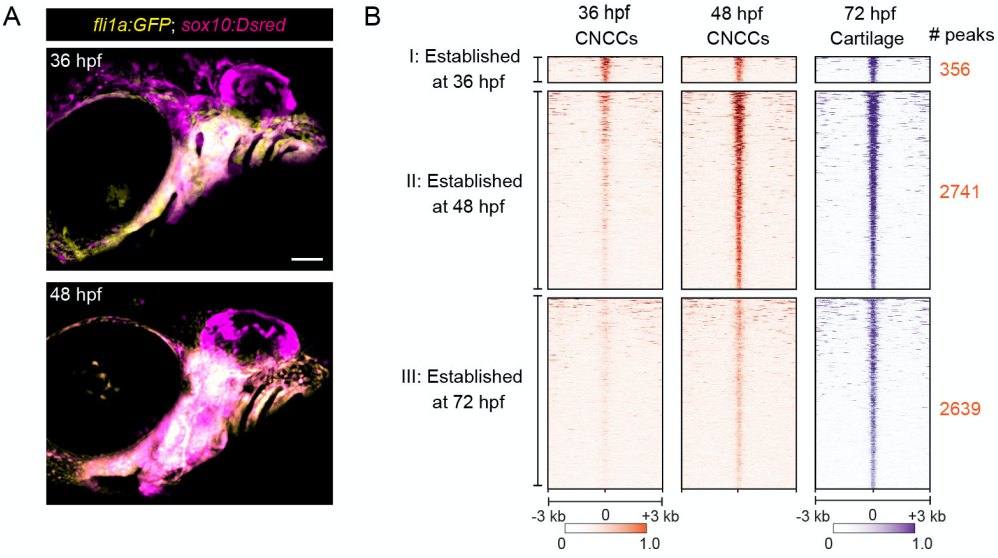

C

	Motif	Best Match TFs	P value
Group I		Nfat	1e-24
		Foxa2	1e-23
		Lhx	1e-21
		Nr2f	1e-18
		Meis	1e-17
		Pax	1e-17

D

GO Term	P value
Regulation of transcription	6.5e-5
Vasculature development	6.2e-4
Neural crest cell migration	9.2e-4
Mesoderm cell migration	1.0e-3
Cell migration involved in gastrulation	1.3e-3
Dorsal/ventral pattern formation	3.6e-3

E

	Motif	Best Match TFs	P value
Group II		Sox(Dimer)	1e-445
		Foxa1	1e-106
		Nfat	1e-91
		Egr	1e-65
		Ap1	1e-60
		Nkx	1e-58

F

GO Term	P value
Transcription	9.6e-8
Regulation of transcription	1.8e-7
Cell differentiation	4.4e-7
Skeletal system development	3.0e-6
Vasculature development	4.1e-6
Multicellular organism development	5.0e-6

G

	Motif	Best Match TFs	P value
Group III		Nfat	1e-155
		Foxa1	1e-110
		Sox(Dimer)	1e-73
		Ap1	1e-72
		Tead	1e-63
		Irf	1e-54

H

GO Term	P value
Regulation of transcription	1.2e-7
Dorsal/ventral pattern formation	2.3e-6
Cartilage development	6.9e-6
Transcription	1.6e-5
Retinal ganglion cell axon guidance	1.3e-4
Multicellular organism development	1.6e-4

Figure 2. Dynamics of chromatin accessibility across facial chondrogenesis

bioRxiv preprint doi: https://doi.org/10.1101/2020.10.15.340703; this version posted October 15, 2020. The copyright holder for this preprint (which was not certified by peer review) is the author/funder, who has granted bioRxiv a license to display the preprint in perpetuity. It is made available under aCC-BY 4.0 International license.

443 (A) Confocal images of CNCCs expressing *fli1a:GFP* and *sox10:Dsred* at 36 and 48 hpf. Lateral

444 view with anterior to left. Scale bar = 100 μm. (B) Peak intensity plots of cartilage-accessible

445 distal elements shown for chondrocytes at 72 hpf and CNCCs at 36 and 48 hpf. Chondrocyte

446 accessible elements are pooled into three categories based on dynamics of chromatin

447 accessibility across stages. (C, E, G) De novo motif enrichment recovered by Homer analysis

448 among the three categories. Top 6 motifs are shown with associated P values after removing

449 redundant motifs. (D, F, G) GO term analysis among the three categories.

450

bioRxiv preprint doi: https://doi.org/10.1101/2020.10.15.340703; this version posted October 15, 2020. The copyright holder for this preprint (which was not certified by peer review) is the author/funder, who has granted bioRxiv a license to display the preprint in perpetuity. It is made available under aCC-BY 4.0 International license.

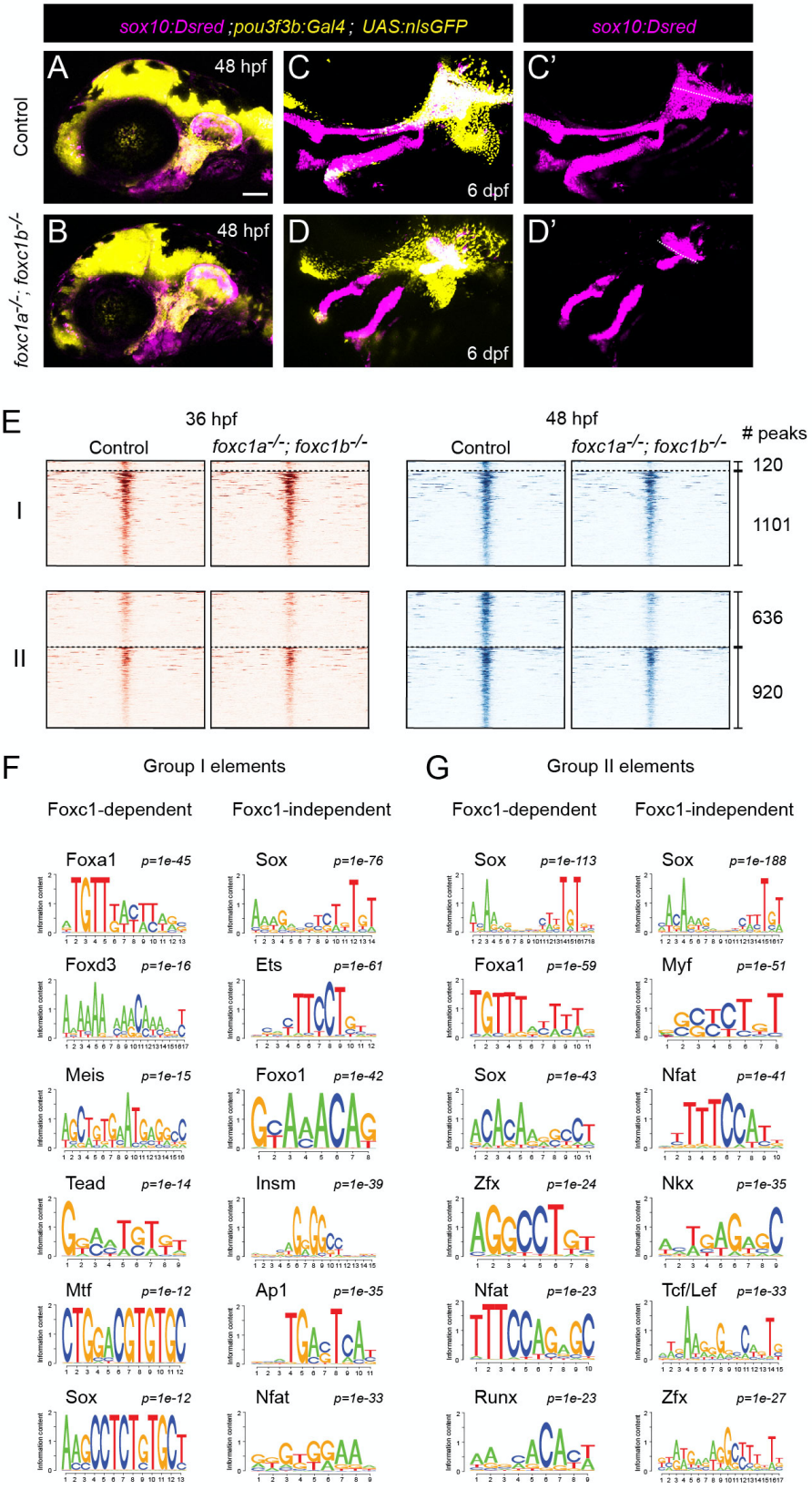

Figure 3. Foxc1 dependency of facial chondrocyte chromatin accessibility

bioRxiv preprint doi: https://doi.org/10.1101/2020.10.15.340703; this version posted October 15, 2020. The copyright holder for this preprint (which was not certified by peer review) is the author/funder, who has granted bioRxiv a license to display the preprint in perpetuity. It is made available under aCC-BY 4.0 International license.

453 (A, B) Confocal images show dorsal CNCCs of the first two arches labeled by *sox10:Dsred* and

454 *pou3f3b:Gal4*; *UAS:nlsGFP* in control and *foxc1a*$^{-/-}$; *foxc1b*$^{-/-}$ mutant embryos at 48 hpf. Scale

455 bar = 100μm. (C, D) Confocal images show loss of dorsal cartilages in *foxc1a*$^{-/-}$; *foxc1b*$^{-/-}$ mutant

456 embryos at 6 dpf. *sox10:Dsred*+ cartilages are seen in single channels in C' and D', with dashed

457 lines highlighting boundaries of dorsal and otic cartilage. (E) Peak intensity plots of Group I and

458 Group II elements in control and *foxc1a*$^{-/-}$; *foxc1b*$^{-/-}$ mutant embryos. Peaks above the dashed

459 lines are reduced in mutants. (F, G) De novo motif enrichment of Foxc1-dependent and Foxc1-

460 independent Group I and Group II elements. Top 6 motifs are shown with associated P values

461 after removing redundant motifs.

462

bioRxiv preprint doi: https://doi.org/10.1101/2020.10.15.340703; this version posted October 15, 2020. The copyright holder for this preprint (which was not certified by peer review) is the author/funder, who has granted bioRxiv a license to display the preprint in perpetuity. It is made available under aCC-BY 4.0 International license.

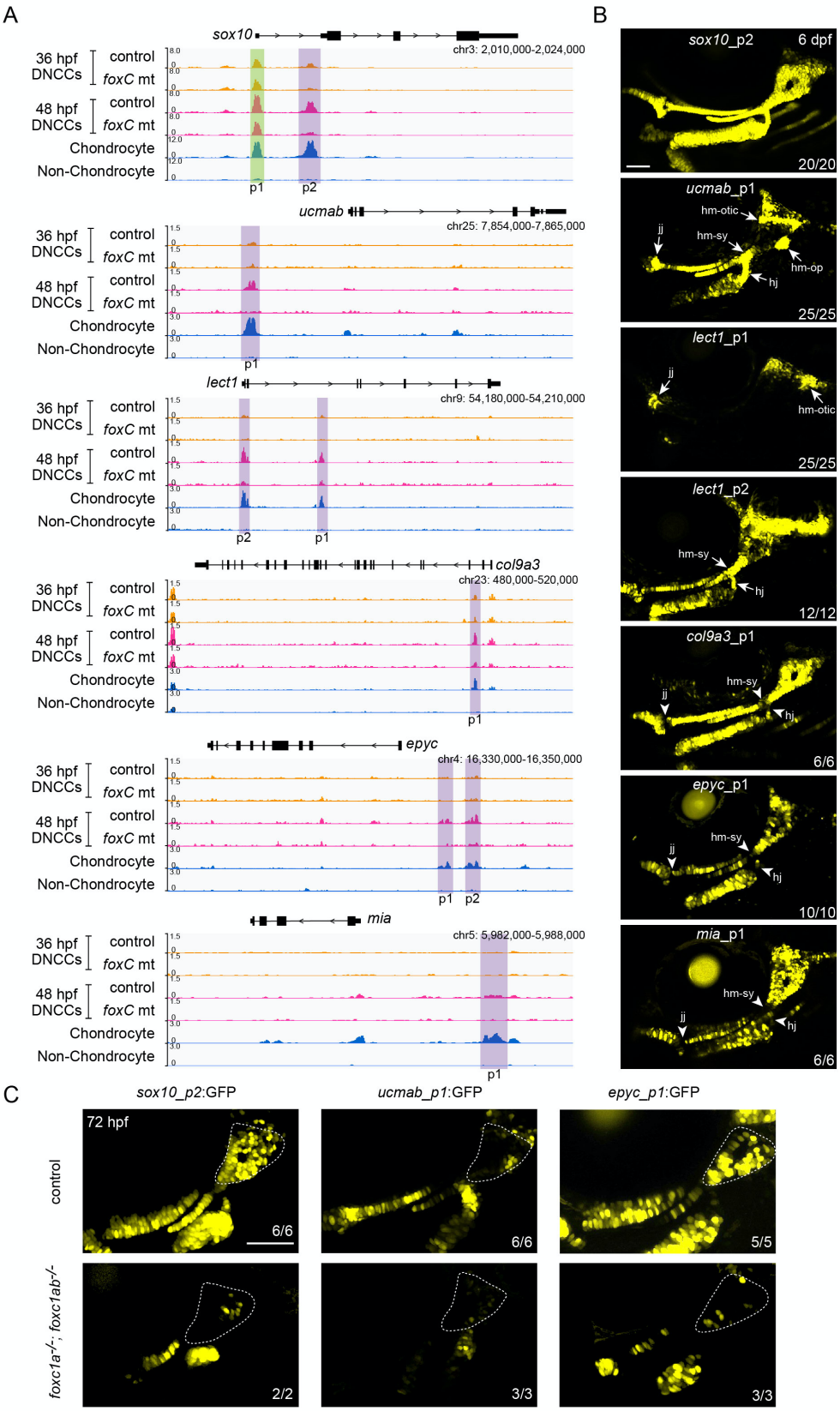

bioRxiv preprint doi: https://doi.org/10.1101/2020.10.15.340703; this version posted October 15, 2020. The copyright holder for this preprint (which was not certified by peer review) is the author/funder, who has granted bioRxiv a license to display the preprint in perpetuity. It is made available under aCC-BY 4.0 International license.

Figure 4. In vivo validation of Foxc1-dependent cartilage enhancers

(A) Snapshots of genomic regions (genes and GRCz10 coordinates listed) for enhancer testing. Peaks (p) tested are shown, with Foxc1-dependent regions in purple and a Foxc1-independent element in green. μATACseq reads are shown in each row for the experiments indicated, with chondrocyte and non-chondrocyte peaks from 72 hpf embryos. DNCCs, dorsal CNCCs. (B) GFP expression driven by the indicated peaks in stable transgenic zebrafish at 6 dpf. Confocal projections of the cartilages of the first two arches are shown in lateral view with anterior to the left. Arrows indicate enriched expression at joint regions, and arrowheads denote relative lack of expression. jj, jaw joint. hj, hyoid joint. hm-sy, hyomandibular-symplectic junction. hm-otic, hyomandibular-otic junction. hm-op, hyomandibular-opercular joint. (C) Confocal projections show selective loss of *sox10_p2:EGFP*, *ucmab_p1:EGFP*, and *epyc_p1:EGFP* transgene expression in the dorsal cartilage domains (dashed outlines) of *foxc1a*$^{-/-}$*; foxc1b*$^{-/-}$ mutants at 72 hpf. Numbers indicate proportion of embryos in which the displayed patterns were observed. Scale bars = 100 μm.

bioRxiv preprint doi: https://doi.org/10.1101/2020.10.15.340703; this version posted October 15, 2020. The copyright holder for this preprint (which was not certified by peer review) is the author/funder, who has granted bioRxiv a license to display the preprint in perpetuity. It is made available under aCC-BY 4.0 International license.

480 **SUPPLEMENTARY FIGURE LEGENDS**

481 **Figure 1-figure supplement 1. *col2a1a* enhancer and cartilage motif comparison between**

482 **zebrafish and mouse**

483 (A) Snapshot of the *col2a1a* locus showing μATACseq reads from the indicated experiments.

484 Several regions become accessible in 48 hpf CNCCs and then remain open in chondrocytes at

485 72 hpf. Boxed region shows the published R2 cartilage enhancer. (B) Comparison of consensus

486 motif sequences recovered from zebrafish μATACseq peaks enriched in facial chondrocytes

487 (left) and mouse Sox9 ChIP-Seq peaks in rib chondrocytes (right).

488

489 **Figure 3-figure supplement 1. Comparison of accessible regions between pan- and**

490 **dorsal CNCCs**

491 Venn diagrams and heatmaps show distal accessible elements in μATACseq data from

492 *fli1a:GFP*+; *sox10:Dsred*+ (pan-CNCCs) and *pou3f3b>GFP*+*; sox10:DsRed*+ (dorsal CNCCs) at

493 36 hpf (A) and 48 hpf (B). Numbers list elements unique for each population or shared (center of

494 circles).

495

bioRxiv preprint doi: https://doi.org/10.1101/2020.10.15.340703; this version posted October 15, 2020. The copyright holder for this preprint (which was not certified by peer review) is the author/funder, who has granted bioRxiv a license to display the preprint in perpetuity. It is made available under aCC-BY 4.0 International license.

Figure 3-figure supplement 2. Accessibility of cartilage-enriched elements in earlier pan- and dorsal CNCCs.

(A,B) Heatmaps of the 5,736 distal elements with accessibility in 72 hpf chondrocytes. Their accessibility is then plotted according to μATACseq data from *fli1a:GFP*+; *sox10:Dsred*+ (pan-CNCCs) and *pou3f3b>GFP+; sox10:Dsred*+ (dorsal CNCCs) at 36 hpf (A) and 48 hpf (B). At 36 hpf, 132 peaks were more accessible in pan-CNCCs and 106 peaks more accessible in dorsal CNCCs. At 48 hpf, 2,470 peaks were more accessible in pan-CNCCs and 10 peaks more accessible in dorsal CNCCs. Peaks commonly or not accessible in both data sets are also shown. (C,D) Pearson correlation graphs of the behavior of cartilage-associated distal elements in pan- versus dorsal CNCCs at 36 and 48 hpf. x and y axes represent raw read counts from BAM files, and “r” is the Pearson correlation coefficient.

Figure 4-figure supplement 1. Additional in vivo validation of cartilage-enriched accessible elements

(A) Schematic of the reporter construct for enhancer testing. Tol2, transposase integration site. E1b, minimal promoter. GFP, green fluorescent protein. pA, polyadenylation sequence. CFP,

bioRxiv preprint doi: https://doi.org/10.1101/2020.10.15.340703; this version posted October 15, 2020. The copyright holder for this preprint (which was not certified by peer review) is the author/funder, who has granted bioRxiv a license to display the preprint in perpetuity. It is made available under aCC-BY 4.0 International license.

512 cerulean fluorescent protein. (B) Snapshots of genomic regions (genes and GRCz10

513 coordinates listed) for enhancer testing. Peaks (p) tested are shown, with Foxc1-dependent

514 regions in purple and Foxc1-independent elements in green. μATACseq reads are shown in

515 each row for the experiments indicated, with chondrocyte and non-chondrocyte peaks from 72

516 hpf embryos. DNCCs, dorsal CNCCs. (C) GFP expression (yellow) driven by the indicated

517 peaks in stable transgenic zebrafish at 6 dpf. Confocal projections of the cartilages of the first

518 two arches are shown in lateral view for *acan_p1* and ventral view for *col9a1a_p1*. For *acan_p1*,

519 *sox10:Dsred* labels all chondrocytes for reference in magenta, and arrow indicates hyoid joint

520 expression. For *col9a1a_p1*, arrows indicate expression in the ventral Meckel's and ceratohyal

521 cartilages. (D) Confocal sections of representative embryos injected with enhancer constructs

522 are shown in lateral view at 6 dpf. Mosaic expression in chondrocytes (yellow, arrows) is shown

523 with DIC providing embryo context in white. For *sparc_p1*, interopercular ligament expression is

524 denoted by arrowhead. Numbers indicate proportion of embryos in which the displayed patterns

525 were observed. Scale bar = 100 μm.

A

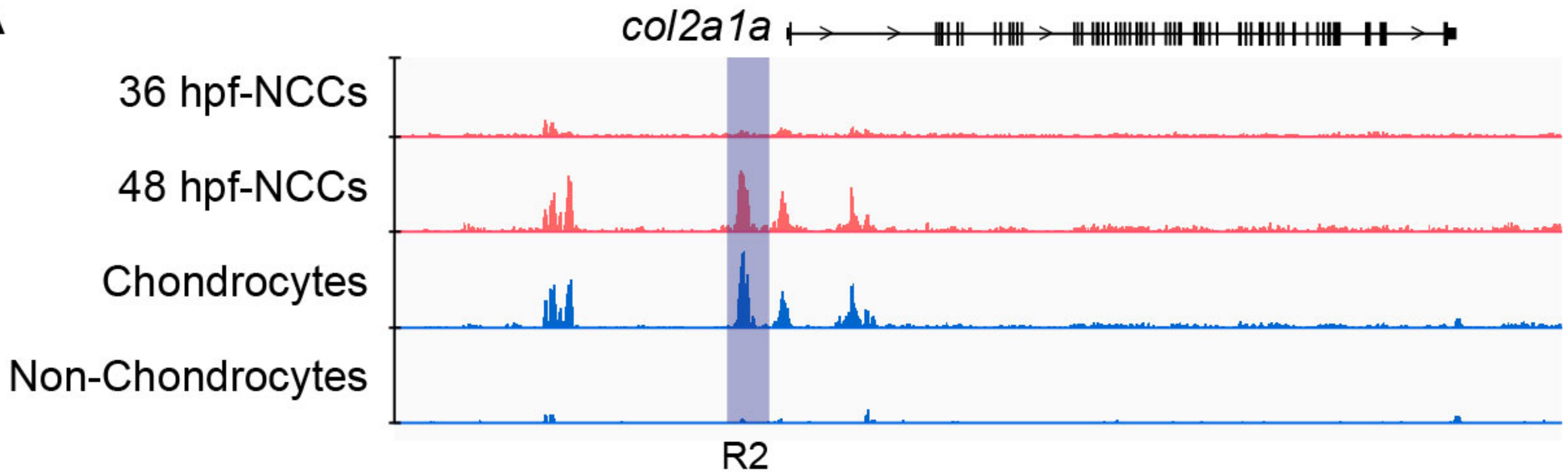

bioRxiv preprint doi: https://doi.org/10.1101/2020.10.15.340703; this version posted October 15, 2020. The copyright holder for this preprint (which was not certified by peer review) is the author/funder, who has granted bioRxiv a license to display the preprint in perpetuity. It is made available under aCC-BY 4.0 International license.

B

Zebrafish motif sequences	Mouse motif sequences (Ohba et al., 2015)
Sox	Sox
Fox	Fox
Nfat	Nfat

A

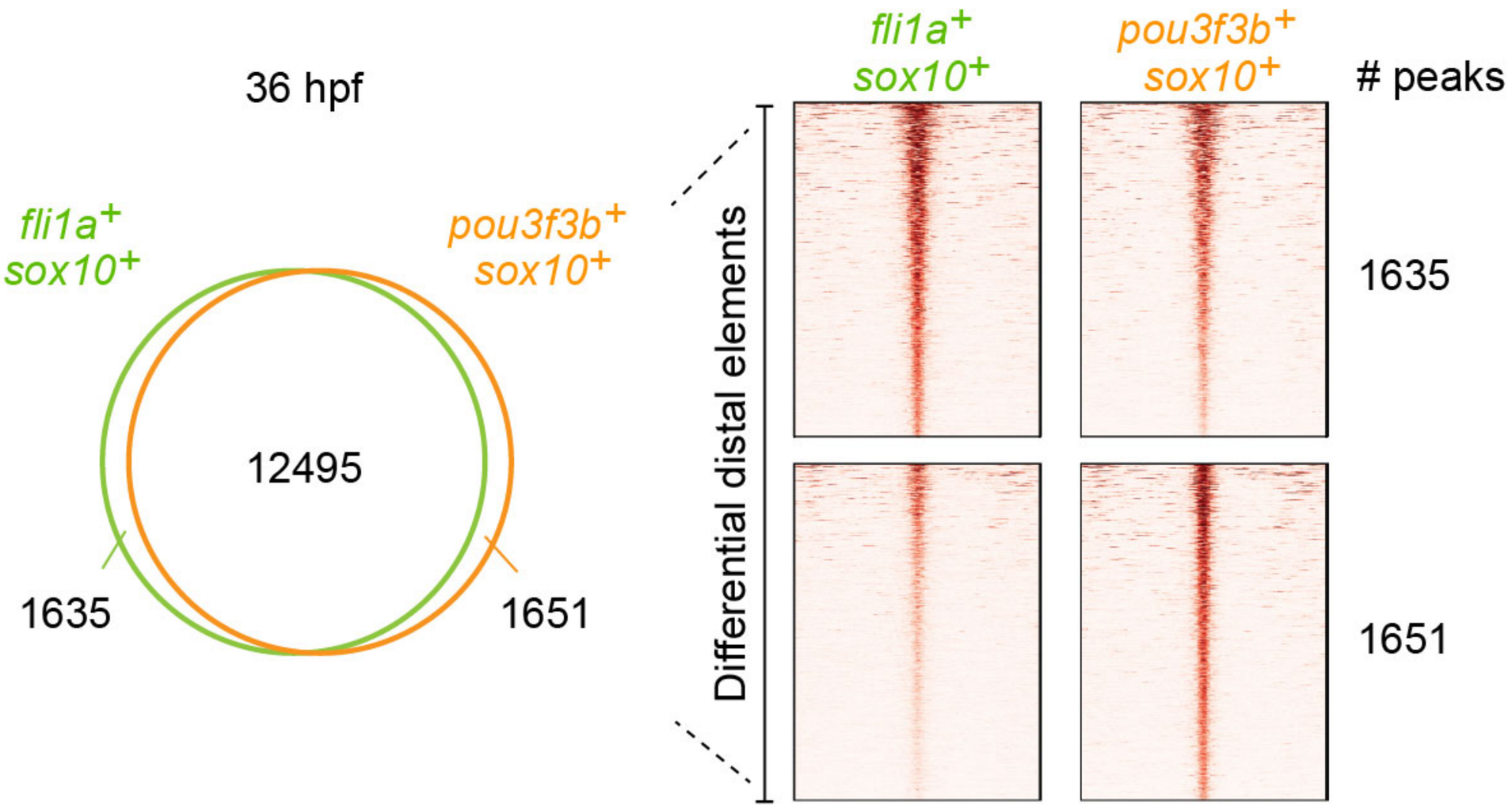

bioRxiv preprint doi: https://doi.org/10.1101/2020.10.15.340703; this version posted October 15, 2020. The copyright holder for this preprint (which was not certified by peer review) is the author/funder, who has granted bioRxiv a license to display the preprint in perpetuity. It is made available under aCC-BY 4.0 International license.

B

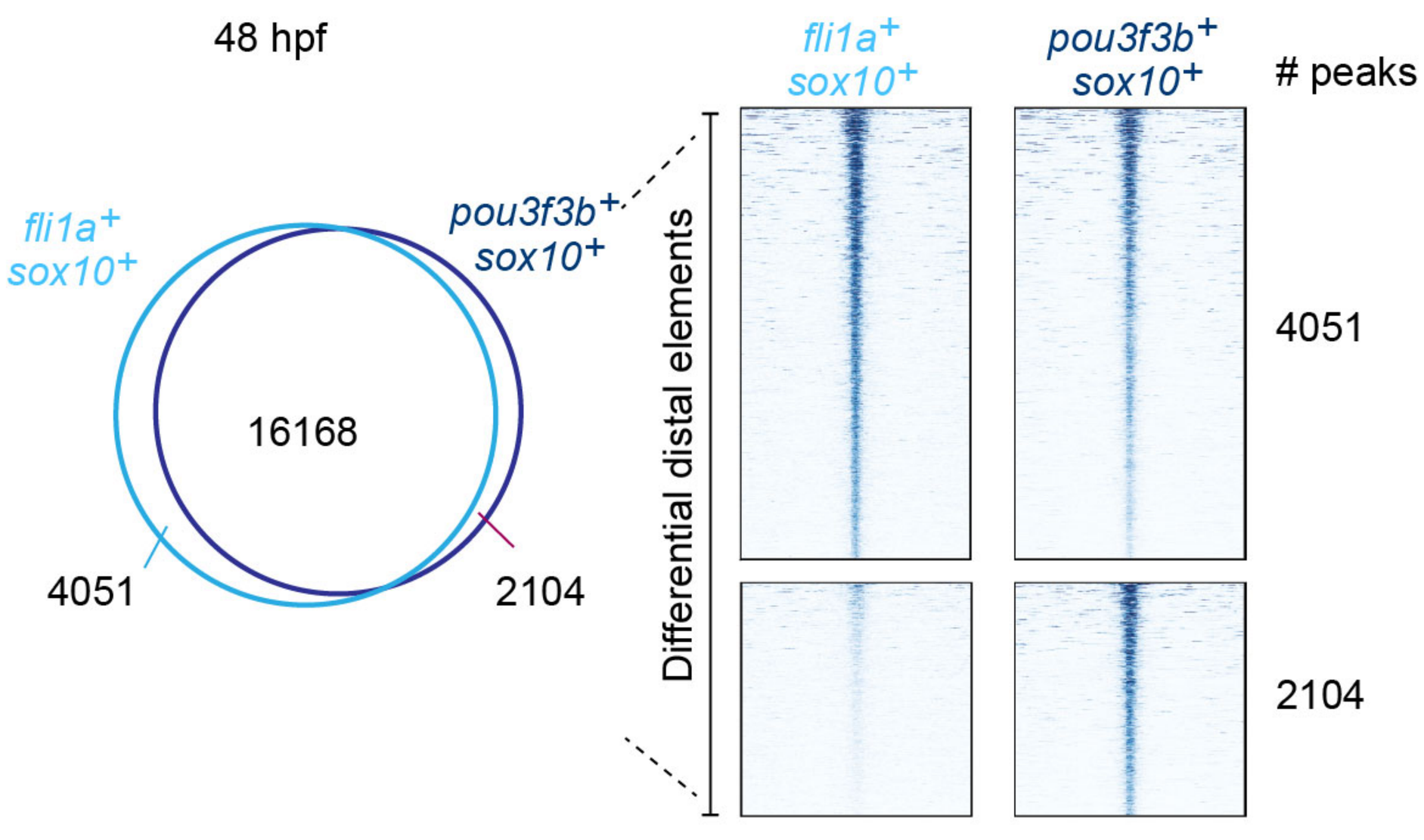

bioRxiv preprint doi: https://doi.org/10.1101/2020.10.15.340703; this version posted October 15, 2020. The copyright holder for this preprint (which was not certified by peer review) is the author/funder, who has granted bioRxiv a license to display the preprint in perpetuity. It is made available under aCC-BY 4.0 International license.

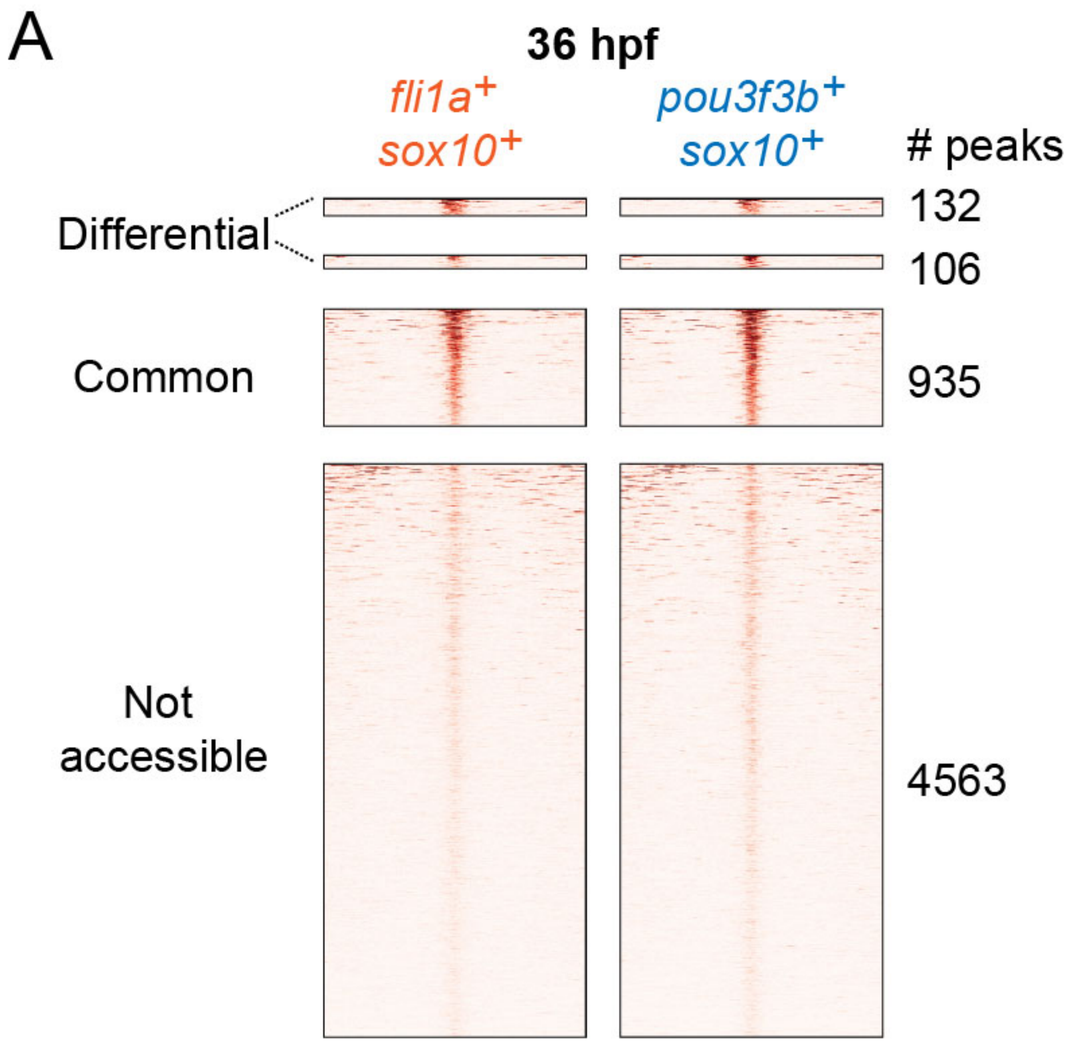

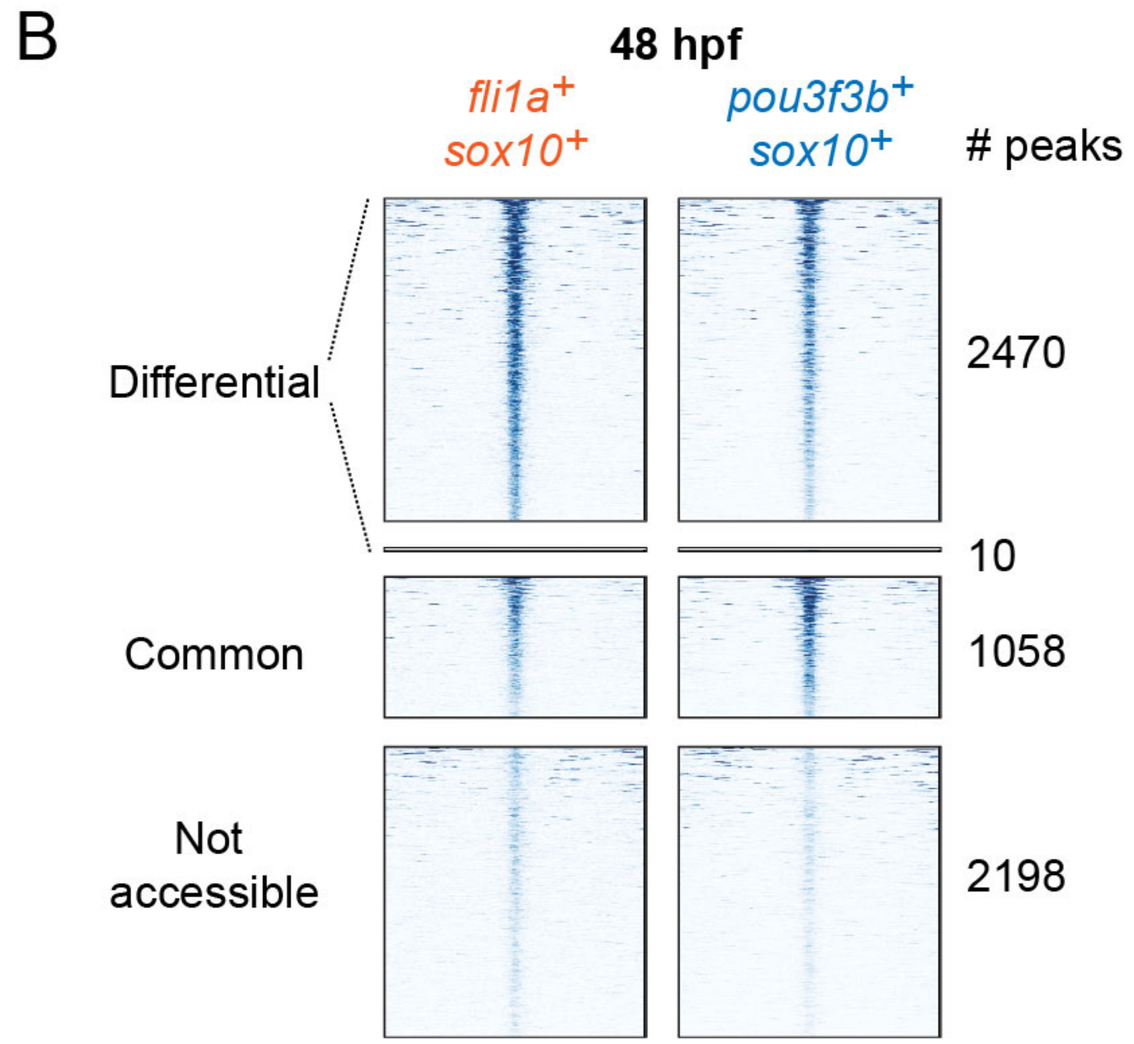

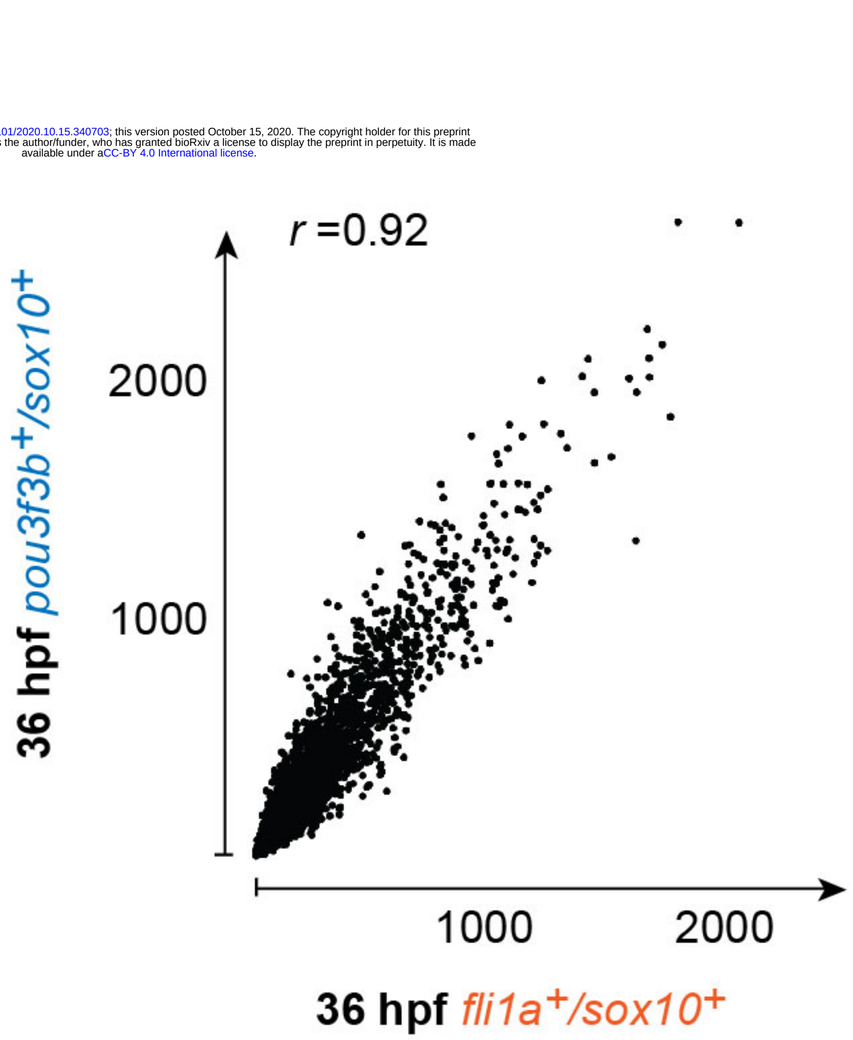

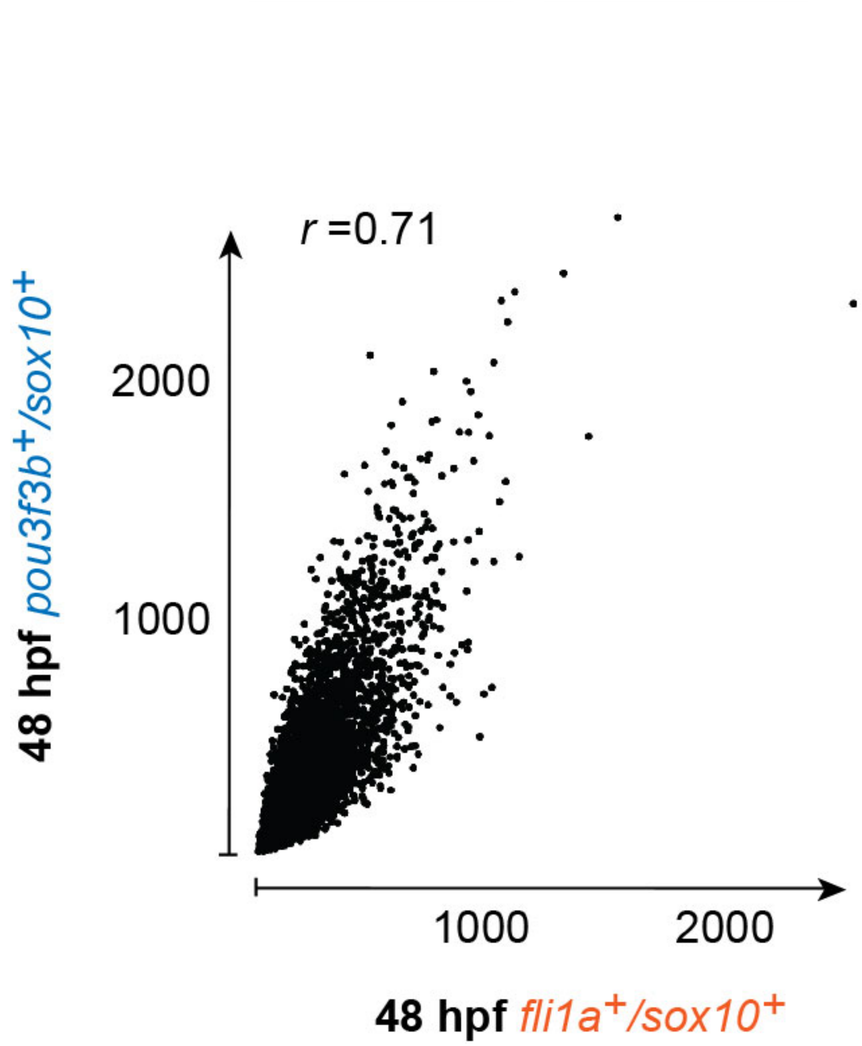

A

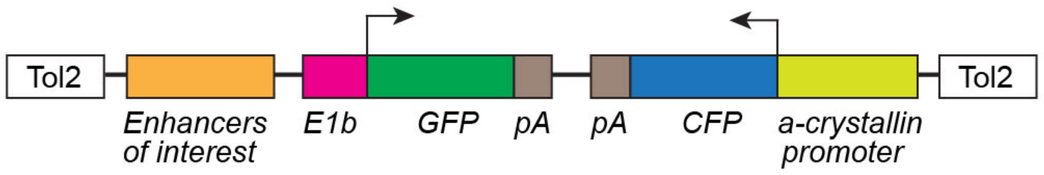

B

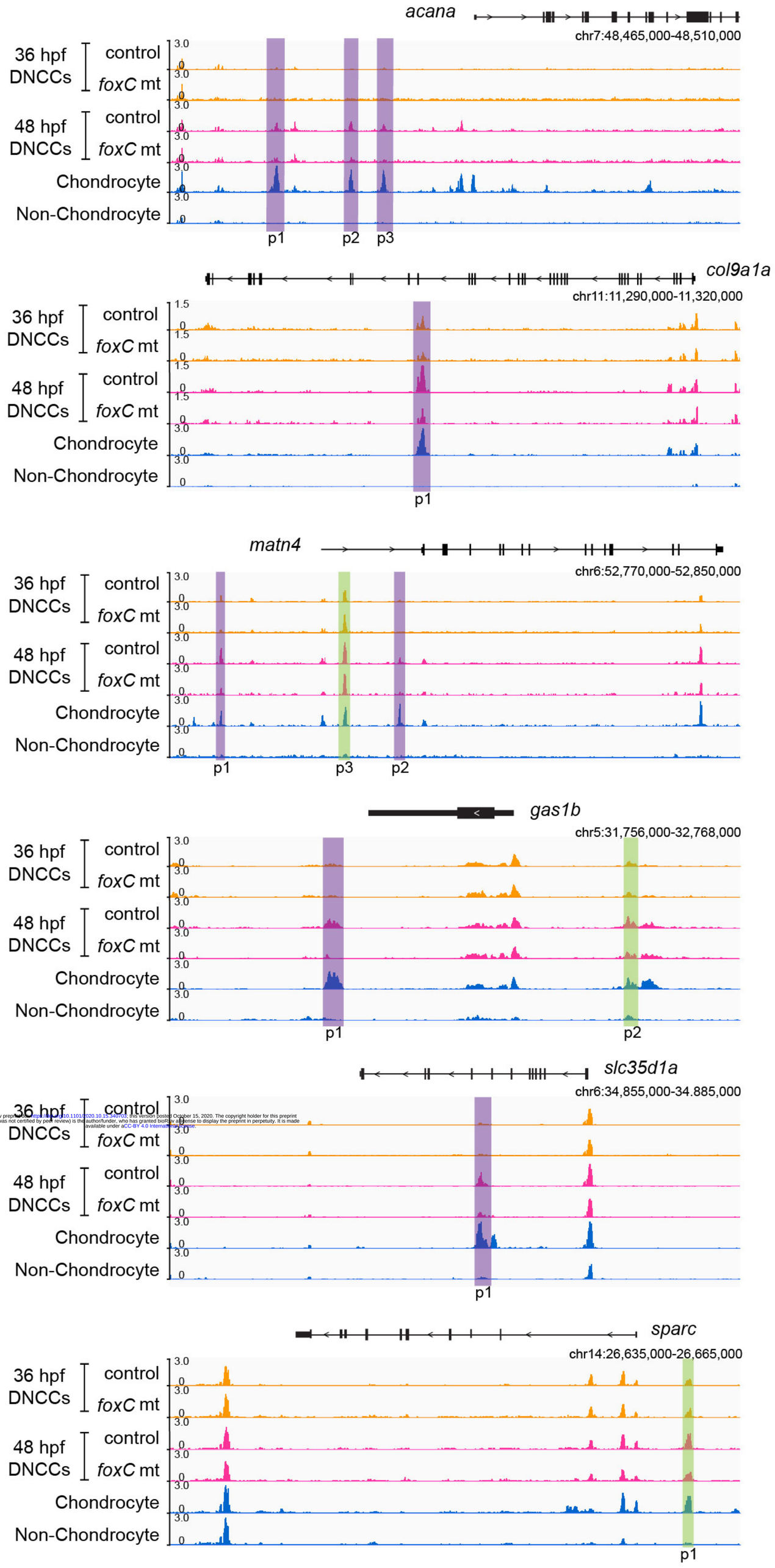

C

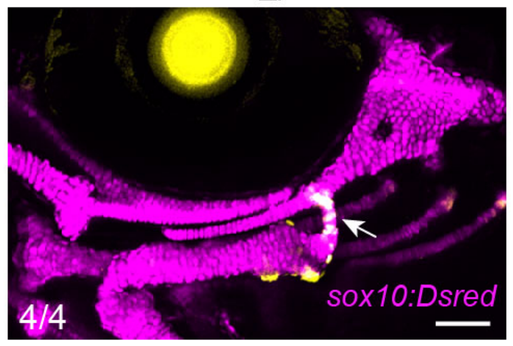

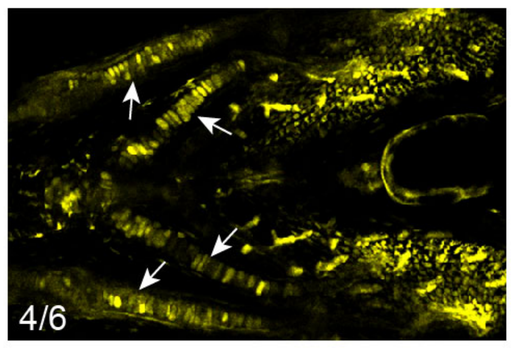

D

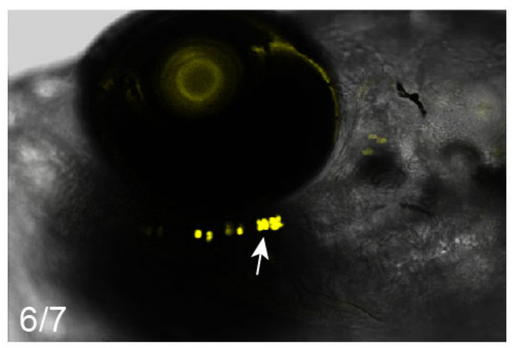

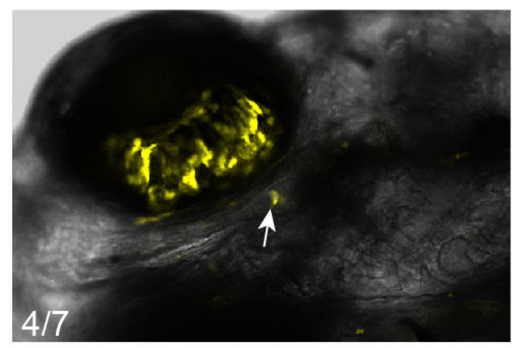

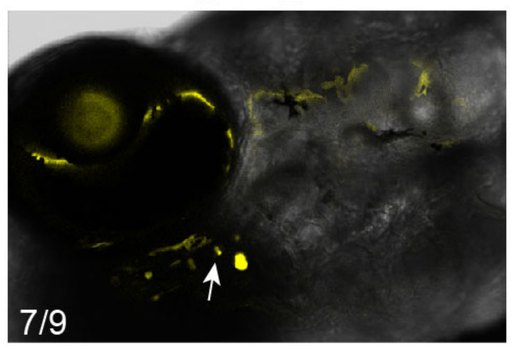

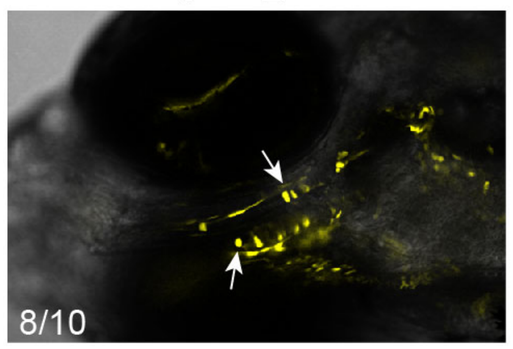

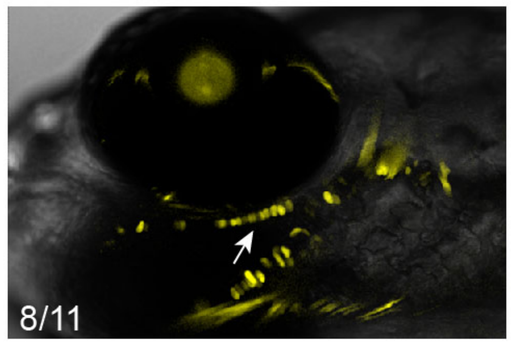

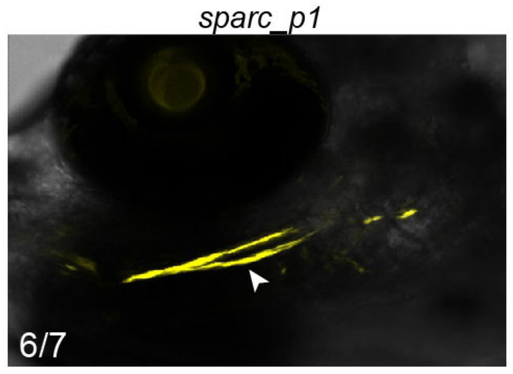

bioRxiv preprint doi: https://doi.org/10.1101/2020.10.15.340703; this version posted October 15, 2020. The copyright holder for this preprint (which was not certified by peer review) is the author/funder, who has granted bioRxiv a license to display the preprint in perpetuity. It is made available under aCC-BY 4.0 International license.